Section 1

Direct collider search of WIMPs

In this section, we review the production of TeV-scale WIMPs and search for their signals using the collider experiment. In particular, we will summarize the current bounds for WIMPs obtained at the large hadron collider (LHC) and future bounds expected at the future planned 100 TeV colliders such as the hadron option of the future circular collider (FCC-hh) [1] and the super proton-proton collider (SPPC) [2,3]. In Sec. 1.1, we discuss the dominant production processes of WIMPs at a hadron collider. In Sec. 1.4 and **(♣ ??? ♣)**, we review **(♣ two??? ♣)** different methods for the signal identification, the disappearing track search and mono-jet search **(♣ ??? ♣)**, and summarize the current and future bounds.

1.1 WIMP production

There are two relevant processes both of which significantly contribute to the WIMP production cross section. The pair production via electroweak interaction is a universal process that can be considered for any WIMP considered in this thesis. The decay of colored particles may also be efficient particularly for the MSSM. In this subsection, we will review these two in order.

Pair production via electroweak interaction

Since all the WIMPs considered here possess non-zero $SU(2)_L$ and $U(1)_Y$ charges, they can be directly produced via electroweak interaction at the hadron collider as shown in Fig. 1. [♮1]
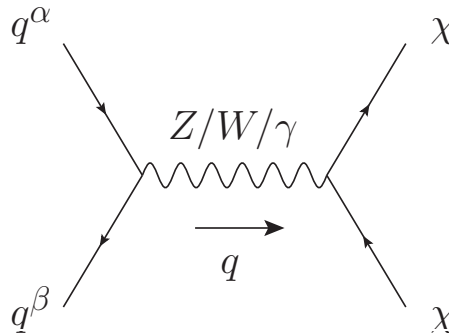

Figure 1: WIMP pair production process at the hadron collider.

[♮1]All the Feynman diagrams in this thesis are drawn with the public code `JaxoDraw-2.1` [4], which is a graphical user interface that allows users to draw Feynman diagrams intuitively and export them in the

In the figure, q^α and q^β denote the partons (namely, one of quarks or gluon) of the incident protons relevant for the process, while χ denotes the WIMP and q is the momentum transfer. Assuming the WIMP to be a $SU(2)_L$ n-plet with $U(1)_Y$ charge Y and the mass m_χ, this process is well described by the effective lagrangian [♮2]

$$\mathcal{L} = \mathcal{L}_{\text{SM}} + (D^\mu \chi)^\dagger (D_\mu \chi) - m_\chi^2 \chi^\dagger \chi \qquad \text{(complex scalar)}, \qquad (1.1)$$

$$\mathcal{L} = \mathcal{L}_{\text{SM}} + \bar{\chi}(i\slashed{D} - m_\chi)\chi \qquad \text{(Dirac fermion)}, \qquad (1.2)$$

with $\mathcal{L}_{\text{SM}}$ being the SM lagrangian, while the covariant derivative is given by

$$D_\mu \equiv \partial_\mu - ig_2 W^a T_n^a - ig_1 Y \slashed{B}, \qquad (1.3)$$

where T_n^a ($a = 1, 2, 3$) are n-dimensional representation matrices of $SU(2)_L$. Note that when χ is a real scalar (Majorana fermion) with $Y = 0$, the terms with χ in Eq. (1.1) (Eq. (1.2)) should be devided by two.

For the calculation, we neglect the effect of the electroweak symmetry breaking, which is valid because we are interested in the high-energy collision with the parton-level center-of-mass (CM) energy $\sqrt{s'} \equiv \sqrt{q^2} \gtrsim \text{TeV}$. Then, we consider the process in the CM frame and estimate the parton-level differential cross section as

$$\left.\frac{d\sigma_{\alpha\beta}}{d\sqrt{s'}d\Omega}\right|_{\text{CM}} = \frac{C_{\alpha\beta}}{8s'}\left(1 - \frac{4m_\chi^2}{s'}\right)^{3/2}\sin^2\theta \qquad \text{(complex scalar)} \qquad (1.4)$$

$$\left.\frac{d\sigma_{\alpha\beta}}{d\sqrt{s'}d\Omega}\right|_{\text{CM}} = \frac{C_{\alpha\beta}}{4s'}\sqrt{1 - \frac{4m_\chi^2}{s'}}\left[1 + \frac{4m_\chi^2}{s'} + \left(1 - \frac{4m_\chi^2}{s'}\right)\cos^2\theta\right] \qquad \text{(Dirac fermion)}, \qquad (1.5)$$

where θ is the angle between the momentum of the initial parton q_a and that of one of the final state WIMPs. These expressions are valid only when the center of mass energy exceeds the production threshold, $\sqrt{s'} > 2m_\chi$. Note also that these expressions represent inclusive cross sections, $i.e.$, the total cross section for the production of any component of the WIMP multiplet χ. The coefficient $C_{\alpha\beta}$ consists of contributions from $U(1)_Y$ and $SU(2)_L$ gauge bosons, [♮3]

$$C_{\alpha\beta} = c_{1\alpha\beta}Y^2\alpha_1^2 + c_{2\alpha\beta}I(n)\alpha_2^2, \qquad (1.6)$$

eps format with the help of the (modification of) `axodraw` style file for LaTeX [5]. Under the environment of macOS Mojave, it apparently fails to start, but one can still execute it by looking inside the application and start the Java executable file `jaxodraw-2.1-0.jar` directly. We would like to thank the authors for providing the best tools to write the thesis with. **(♣ Where is the first place of Feynman diagrams? ♣)**

[♮2]In this subsection, we neglect the small mass difference among different components in the multiplet χ described in 1.4. This approximation is valid since the mass difference is by far smaller than m_χ and has only a tiny effect on the production process.

[♮3]There is no contribution from the interference term between $U(1)_Y$ and $SU(2)_L$ contributions, since it is proportional to $\text{Tr}(T_n^a) = 0$.

with $I(n)$ being the Dynkin index for the n-dimensional representation given by

$$I(n) \equiv \frac{n^3 - n}{12}. \tag{1.7}$$

The explicit form of $c_{1\alpha\beta}$ and $c_{2\alpha\beta}$, which are sizes of the couplings between partons of our choice and gauge bosons, can be expressed using the $U(1)_Y$ charge for a parton Y_α and the $SU(2)_L$ reducible 13-dimensional representation matrices for partons $T^a_{\alpha\beta}$ as

$$c_{1\alpha\beta} = Y^2_\alpha \delta_{\alpha\beta}, \tag{1.8}$$

$$c_{2\alpha\beta} = \sum_a \left| T^a_{\alpha\beta} \right|^2. \tag{1.9}$$

Recalling that $\alpha_1 < \alpha_2$ and that we often consider the WIMPs with large n and moderate Y, the WIMP production cross section grows as n^3 for larger multiplets according to Eq. (1.7).

As is well-known, the initial state of the hadron collider is not the individual partons but two protons. To obtain the cross section for the two protons initial state, we rely on the parton distribution function (PDF), which expresses the fraction of the partons with some given momentum in each accelerated proton. Let $f_a(x)$ ($0 < x < 1$) be the PDF for a given parton a inside a proton with momentum p^μ. $f_a(x)$ can be interpreted as a probability distribution to find the parton a with momentum xp^μ, so we have a relationship

$$\sum_a \int_0^1 dx \, x f_a(x) = 1, \tag{1.10}$$

associated with the total momentum conservation, and

$$\int_0^1 dx \, [f_d(x) - f_{\bar{d}}(x)] = 1, \tag{1.11}$$

$$\int_0^1 dx \, [f_u(x) - f_{\bar{u}}(x)] = 2, \tag{1.12}$$

from the composition of the proton. Using the PDF, the cross section for the process of interest at the hadron collider is evaluated as

$$\frac{d\sigma}{d\sqrt{s'}d\Omega} = \sum_{a,b} \int_0^1 dx_1 dx_2 \, f_a(x_1) f_b(x_2) \delta\left(s' - sx_1 x_2\right) \left. \frac{d\sigma_{ab}}{d\Omega} \right|_{\mathrm{lab}}, \tag{1.13}$$

where $\sqrt{s}$ is the CM energy of the proton-proton collision. Note that the cross section in the integrand is a function of x_1 and x_2, which is obtained by performing the appropriate Lorentz transformation to $d\sigma_{ab}/d\Omega \left.\right|_{\mathrm{CM}}$. (♣ **Comment on factorization scale?** ♣)

Hadron colliders have several more features related to the strong interaction of quantum chromodynamics (QCD). Firstly, the next-to-leading order (NLO) QCD contribution to each

Figure 2: Example of NLO QCD contributions to the WIMP pair production process.

process is not necessarily negligible. For the WIMP pair production, the real and virtual emission of a gluon shown in the left and right panels of Fig. 2, respectively, give the NLO QCD contributions, which will also be taken into account from now on. In particular, when the large transverse momentum is important for the phenomenology of our concern, such as the case in Sec. (♣ ??? ♣), the real emission of a gluon with sizable transverse momentum significantly modifies the calculation. Secondly, all the colored particles in the initial, intermediate, and final states should be accompanied with numbers of soft emissions of gluons, which is the phenomena so-called the parton shower. In practice, there is a difficulty caused by the partial overlap of the gluon phase space between the one-gluon emission cross section considered as an NLO QCD effect and the same considered as the parton shower. To avoid this overlap, we often perform the matching procedure, in which we set some merging energy scale by hand and include the contribution to the cross section with gluon energy above (below) the scale only from the NLO QCD (parton shower) calculation. Finally, the colored particles in the final states should eventually be confined, which is called the hadronization, and observed as some energetic and collimated sprays of hadrons, which as a whole is called jets.

In the following, we perform the numerical calculation, taking account of all the above complexities. For this purpose, we make use of the Monte Carlo generator `MadGraph5 aMC@NLO (v2.6.3.2)` [6, 7] with the successive use of `Pythia8` [8] for the parton shower, hadronization, and matching and `Delphes (v3.4.1)` [9] for the detector simulation, including the definition of jets as observed objects. We use the so-called MLM-style matching [10] with the merging scale of $67.5\,\mathrm{GeV}$ and `NNPDF2.3QED` with $\alpha_3(M_Z) = 0.118$ [11] as a canonical set of PDFs.

In Table 1, we list the production cross sections of various WIMPs via a weak gauge boson exchange at a $\sqrt{s} = 100\,\mathrm{TeV}$ hadron collider. As for the WIMP mass, we use the common value $m = 1\,\mathrm{TeV}$ to compare the cross sections among different choice of quantum numbers. σ_{LO} and σ_{NLO} denote the production cross sections without and with the NLO QCD correction, respectively, while the last line is the so-called K-factor defined as $K =$

WIMP name	Higgsino	Wino	5-plet Majorana fermion	5-plet real scalar
σ_{LO} [fb]	15	52	(♣ ??? ♣)	(♣ ??? ♣)
σ_{NLO} [fb]	17	60	(♣ ??? ♣)	(♣ ??? ♣)
K-factor	1.15	1.15		

Table 1:   Table of pair production cross sections of several types of WIMPs. The CM energy $\sqrt{s} = 100\,\mathrm{TeV}$ is assumed and WIMP masses are set to be $1\,\mathrm{TeV}$.

Wino mass [TeV]	1.0	1.5	2.0	2.9
σ_{LO} [fb]	52	12	4.0	0.86
σ_{NLO} [fb]	60	15	4.7	1.0
K-factor	1.15	1.20	1.19	1.21

Table 2:   Table of pair production cross sections of Wino with several choice of masses. The CM energy $\sqrt{s} = 100\,\mathrm{TeV}$ is assumed.

$\sigma_{\mathrm{NLO}}/\sigma_{\mathrm{LO}}$. From the table, by paying attention to the factor two difference in degrees of freedom between the Dirac (Higgsino) and Majorana (Wino and 5-plet) fermions, we can roughly see the dependence of the cross section on the $SU(2)_L$ charge $\sigma \propto n^3$.   (♣ **Cross section to neutral Higgsino seems missing** ♣)

In Table 2, we also show the mass dependence of the Wino pair production cross section. For heavier mass, wider range of $\sqrt{s'}$ is below the production threshold $2m_\chi$ or accompanied with a small suppression factor $(1 - 4m_\chi^2/s')^{1/2}$ as shown in Eq. (1.5), and the cross section becomes significantly smaller. However, values in the tables still denote that plenty of well-motivated WIMP DM candidates, such as $1\,\mathrm{TeV}$ Higgsino and $3\,\mathrm{TeV}$ Wino, are produced at, for example, the $3\,\mathrm{ab}^{-1}$ option of the FCC-hh.

In Fig. 3, we show the $\sqrt{s'}$ distribution for the pair production process of the $m_\chi = 1\,\mathrm{TeV}$ Higgsino. We assume the setup $\sqrt{s} = 100\,\mathrm{TeV}$ and the integrated luminosity $\mathcal{L} = 3\,\mathrm{ab}^{-1}$. At around $\sqrt{s'} \sim 2m_\chi$, we clearly see the production threshold and the suppression effect $\sigma \propto (1 - 4m_\chi^2/s')^{1/2}$. On the other hand, when $\sqrt{s'}$ becomes much larger than $2m_\chi$, we can see the correct behavior of the cross section, which decreses as $\sigma \propto (\sqrt{s'})^{-3}$ as Eq. (1.5) indicates. Note that these properties are universal among several processes, including the dominant contribution (♣ **Correct?** ♣) to the gluino pair production through the s-channel gluon exchange disscused in the next subsection, and the lepton pair production through via an electroweak gauge boson that is the main topics in Sec. (♣ ??? ♣).

(♣ **Histogram of angular dependence** ♣)

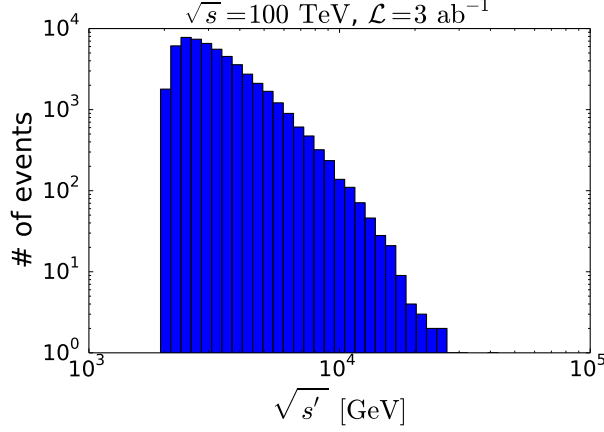(♣ **Is angular dependence affected by the Lorentz boost?** ♣)

Figure 3:   Histogram of the $\sqrt{s'}$ distribution, taking 1 TeV Higgsino as an example. $\sqrt{s} = 100$ TeV and $\mathcal{L} = 3\,\mathrm{ab}^{-1}$ are assumed.

gluino mass [TeV]	6.0	7.0	8.0
$\sigma(pp \to \tilde{g}\tilde{g})$ [fb]	7.9	2.7	1.0

Table 3: Gluino pair production cross section at $\sqrt{s} = 100$ TeV.

Decay of colored particles

In hadron colliders, particles with color charges have far more chance to be produced than non-colored particles. When we consider the split SUSY or the anomaly mediation model reviewed in Sec. **??**, gluino tends to be relatively light, whose decay produces WIMPs. Without fine-tuning of Higgsino and gaugino masses, gluino lifetime is sufficiently short and only its decay products are observed by the detectors. Since all the SUSY particles finally decay into the LSP as described in Sec. **??**, the gluino production cross section can effectively be counted as the production cross section of WIMPs in these models.

Keeping the R-parity conservation in our mind, the dominant process accompanied with gluinos in these models is the gluino pair production. In Table 3, we summarize the gluino pair production cross section for various gluino masses at $\sqrt{s} = 100$ TeV, taken from [12]. The calculation is again performed using `MadGraph5 aMC@NLO` and only the LO QCD processes are considered. The values in the table show that the gluino pair production process, dependeing on its mass, may give much larger cross section for the WIMP production than the purely electroweak processes described above.

(♣ Comment on AMSB $m_{3/2}$ and L for the table? ♣)

1.2   Disappearing track search

Mass splitting among an $SU(2)_L$ multiplet

So far we have neglected the effect from the electroweak symmetry breaking and treated every component of an $SU(2)_L$ multiplet equally. However, in the reality, spontaneously breaking of the $SU(2)_L$ symmetry occurs and this results in the mass splitting among an $SU(2)_L$ multiplet as we will see from now on.

First, we consider the mass splitting caused by the tree-level propagation of heavy particles, such as the SUSY particles other than the LSP, or another unknown particles. After integrating out all the heavy particles other than the SM particles and the light WIMP, we may obtain operators of the form of $\mathcal{O} = M_{ij}\chi_i\chi_j$, where χ denotes the WIMP and i is the $SU(2)_L$ index. This operator causes the mass splitting only when M_{ij} transforms non-trivially under the $SU(2)_L$ symmetry. Then, we can explicitlly construct the lowest dimensional operator among those relevant for the mass splitting. For Higgsino,

$$\mathcal{O} = \frac{1}{\Lambda}(\bar{\chi}H^*)(H\chi), \tag{1.1}$$

where $\chi = (\tilde{H}_u, -i\sigma_2\tilde{H}_d^*)^t$, Φ is the SM Higgs doublet with $Y = 1/2$, Λ is the cut-off scale of the effective theory, *i.e.*, the typical mass scale of the relevant heavy particles, and the parenthesis denotes the $SU(2)_L$ invariant product of fundamental representations. Similarly, for Wino, [13]

$$\mathcal{O} = \frac{1}{\Lambda^3}(H^\dagger\sigma^a H)(H^\dagger\sigma^b H)\tilde{W}^a\tilde{W}^b, \tag{1.2}$$

and higher dimensional operators for MDMs with $n \simeq 5$, as is easily anticipated. A simple implication of this observation is that, for multiplets with large n, there are suppression factors that keeps the tree-level mass splitting small. Already for Wino, the suppression is of $\mathcal{O}(m_W^4)$, which yields a splitting smaller than $10\,\text{MeV}$ for heavy paritlces with a few TeV masses. This is the main reason why the loop correction plays more important role for the mass splitting of Wino and MDMs.

(♣ **Histogram of surviving probability** ♣)
(♣ **Histogram of beta distribution before / after 10cm cut** ♣)

1.3   Soft lepton search

(♣ **If possible** ♣)

1.4   Mono-jet search

References

[1] M. Benedikt, M. Capeans Garrido, F. Cerutti, B. Goddard, J. Gutleber, J. M. Jimenez, M. Mangano, V. Mertens, J. A. Osborne, T. Otto, J. Poole, W. Riegler, D. Schulte, L. J. Tavian, D. Tommasini, F. Zimmermann, Future Circular Collider, Tech. Rep. CERN-ACC-2018-0058, CERN, Geneva, submitted for publication to Eur. Phys. J. ST. (Dec 2018).
URL https://cds.cern.ch/record/2651300

[2] M. Ahmad, et al., CEPC-SPPC Preliminary Conceptual Design Report. 1. Physics and Detector (2015).

[3] C.-S. S. Group, CEPC-SPPC Preliminary Conceptual Design Report. 2. Accelerator (2015).

[4] D. Binosi, J. Collins, C. Kaufhold, L. Theussl, Jaxodraw: A graphical user interface for drawing feynman diagrams. version 2.0 release notes, Computer Physics Communications 180 (9) (2009) 1709 – 1715. doi:https://doi.org/10.1016/j.cpc.2009.02.020.
URL http://www.sciencedirect.com/science/article/pii/S0010465509000757

[5] J. Vermaseren, Axodraw, Computer Physics Communications 83 (1) (1994) 45 – 58. doi:https://doi.org/10.1016/0010-4655(94)90034-5.
URL http://www.sciencedirect.com/science/article/pii/0010465594900345

[6] J. Alwall, M. Herquet, F. Maltoni, O. Mattelaer, T. Stelzer, MadGraph 5 : Going Beyond, JHEP 06 (2011) 128. arXiv:1106.0522, doi:10.1007/JHEP06(2011)128.

[7] J. Alwall, R. Frederix, S. Frixione, V. Hirschi, F. Maltoni, O. Mattelaer, H. S. Shao, T. Stelzer, P. Torrielli, M. Zaro, The automated computation of tree-level and next-to-leading order differential cross sections, and their matching to parton shower simulations, JHEP 07 (2014) 079. arXiv:1405.0301, doi:10.1007/JHEP07(2014)079.

[8] T. Sjöstrand, S. Ask, J. R. Christiansen, R. Corke, N. Desai, P. Ilten, S. Mrenna, S. Prestel, C. O. Rasmussen, P. Z. Skands, An Introduction to PYTHIA 8.2, Comput. Phys. Commun. 191 (2015) 159–177. arXiv:1410.3012, doi:10.1016/j.cpc.2015.01.024.

[9] J. de Favereau, C. Delaere, P. Demin, A. Giammanco, V. Lemaître, A. Mertens, M. Selvaggi, DELPHES 3, A modular framework for fast simulation of a generic collider experiment, JHEP 02 (2014) 057. `arXiv:1307.6346`, `doi:10.1007/JHEP02(2014)057`.

[10] M. L. Mangano, M. Moretti, F. Piccinini, M. Treccani, Matching matrix elements and shower evolution for top-quark production in hadronic collisions, JHEP 01 (2007) 013. `arXiv:hep-ph/0611129`, `doi:10.1088/1126-6708/2007/01/013`.

[11] R. D. Ball, V. Bertone, S. Carrazza, L. Del Debbio, S. Forte, A. Guffanti, N. P. Hartland, J. Rojo, Parton distributions with QED corrections, Nucl. Phys. B877 (2013) 290–320. `arXiv:1308.0598`, `doi:10.1016/j.nuclphysb.2013.10.010`.

[12] S. Asai, S. Chigusa, T. Kaji, T. Moroi, M. Saito, R. Sawada, J. Tanaka, K. Terashi, K. Uno, Studying gaugino masses in supersymmetric model at future 100 TeV pp collider, JHEP 05 (2019) 179. `arXiv:1901.10389`, `doi:10.1007/JHEP05(2019)179`.

[13] T. Gherghetta, G. F. Giudice, J. D. Wells, Phenomenological consequences of supersymmetry with anomaly induced masses, Nucl. Phys. B559 (1999) 27–47. `arXiv:hep-ph/9904378`, `doi:10.1016/S0550-3213(99)00429-0`.